Title	Double-Network Hydrogels Strongly Bondable to Bones by Spontaneous Osteogenesis Penetration
Author(s)	Nonoyama, Takayuki; Wada, Susumu; Kiyama, Ryuji; Kitamura, Nobuto; Mredha, Md Tariful Islam; Zhang, Xi; Kurokawa, Takayuki; Nakajima, Tasuku; Takagi, Yasuaki; Yasuda, Kazunori; Gong, Jian Ping
Citation	Advanced Materials, 28(31), 6740-6745 https://doi.org/10.1002/adma.201601030
Issue Date	2016-08-17
Doc URL	http://hdl.handle.net/2115/62686
Rights(URL)	http://creativecommons.org/licenses/by-nc-nd/4.0/
Type	article
File Information	Nonoyama_et_al-2016-Advanced_Materials.pdf

Instructions for use

COMMUNICATION

Double-Network Hydrogels Strongly Bondable to Bones by Spontaneous Osteogenesis Penetration

Takayuki Nonoyama, Susumu Wada, Ryuji Kiyama, Nobuto Kitamura, Md. Tariful Islam Mredha, Xi Zhang, Takayuki Kurokawa, Tasuku Nakajima, Yasuaki Takagi, Kazunori Yasuda,* and Jian Ping Gong*

Recent progress in developing tough hydrogels has made these highly water-containing materials promising substitutes of soft supporting tissues such as cartilage and ligaments. However, bonding of tough hydrogels to bone is a great challenge for such potential applications. Here, we have developed a novel tough double-network hydrogel that spontaneously bonds to defected bones robustly in vivo. Osteointegration of the hydrogel is realized by mineralizing calcium-phosphate-hydroxide salt hydroxyapatite (HAp) nanospheres in the surface layer of the hydrogel to induce spontaneous osteogenesis penetration into the semipermeable hydrogel. A gel/bone hybrid layer of around 40 μm thickness was observed to give the robust bonding. This is the first success in realizing robust osteointegration of tough hydrogels, and the method is simple and feasible for practical use. This work will be a breakthrough for the potential application of tough hydrogels as substitutes of soft supporting tissues.

The soft supporting tissues in the human body, such as cartilage and ligaments, are tough and firmly fixed to bones. These soft tissues, once injured, cannot regenerate spontaneously in vivo.[1,2] Therefore, artificial supporting tissues would substantially improve outcomes after soft-tissue injury. However, to date, no materials have been developed that are sufficiently tough, yet soft and flexible, for bonding to bone. Recently developed tough hydrogels are promising materials as substitutes of soft supporting tissues.[3–5] However, bonding of hydrogels to other surfaces is difficult because the main component of hydrogels is water.[6,7] Indeed, hydrogels usually have poor adhesion and show low sliding friction on solids.[8] Bonding of tough hydrogels to bones is one of the challenges for potential application of hydrogel materials as soft supporting tissues.

Bone, consisting of proteins and minerals, is a dynamic tissue that is constantly regenerated by osteoblasts and resorbed by osteoclasts, which is called bone remodelling.[9] Osteoclasts secrete acid and collagenase to disassemble bone at a molecular level, and osteoblasts release proteins (mainly collagen), which are crosslinked by deposition of the calcium-phosphate-hydroxide salt HAp to form bone.[9] It is known that synthetically formed HAp has high osteoconduction.[10–13] Thus, a layer of HAp has been coated on the surfaces of solid materials for medical implants to support osteointegration.[10] HAp with a low crystallinity, which can be obtained in mild reaction, shows good bioabsorbability and supports efficient osteogenesis.[11–13]

Hydrogels are semi-permeable to small molecules and ions due to their high water content.[6,7] The semi-permeability makes it possible to mineralize HAp nanocrystals in hydrogels.[14] In addition, hydrogels are also permeable to some proteins, depending on the relative size of the protein to the gel. For example, biosynthesized collagen molecules that have ≈1.5 nm diameter and ≈300 nm length in the triple-helix form[15] are expected to be permeable in hydrogels that usually have a mesh size larger than several nanometers by the reputational motion.[16] Thereby, one can expect biomineralization-like processes to occur inside the gel matrix, even if the osteoblasts and osteoclasts are too large to penetrate into the gel.

Thus, our strategy to bond a tough hydrogel to bone is to spontaneously induce the formation of a gel/bone hybrid layer at the gel–bone interface in vivo, combining the features of the semi-permeability of the hydrogels, the high osteoconductivity of HAp, and the dynamic nature of the bone tissues. For this purpose, we hybridized HAp nanocrystals on the surface layer of a tough double-network hydrogel (DN gel). We found that the HAp-containing gel, denoted as HAp/DN gel, formed robust bonding with defected bones after four weeks implantation, while the pristine DN gel did not. The strong osteointegration

Dr. T. Nonoyama, Dr. T. Kurokawa,
Dr. T. Nakajima, Prof. J. P. Gong
Faculty of Advanced Life Science
Hokkaido University
Sapporo 060-0810, Japan
E-mail: gong@mail.sci.hokudai.ac.jp
Dr. T. Nonoyama, Dr. T. Kurokawa,
Dr. T. Nakajima, Prof. J. P. Gong
Global Station for Soft Matter
Global Institution for Collaborative Research and Education
Hokkaido University
Sapporo 060-0810, Japan
Dr. S. Wada, Dr. N. Kitamura, Prof. K. Yasuda
Department of Sports Medicine and Joint Surgery
Graduate School of Medicine
Hokkaido University
Sapporo 060-0810, Japan
E-mail: yasukaz@med.hokudai.ac.jp
R. Kiyama, Dr. Md. T. I. Mredha
Graduate School of Life Science
Hokkaido University
Sapporo 060-0810, Japan
Dr. X. Zhang, Prof. Y. Takagi
Faculty of Fisheries Science
Hokkaido University
Hakodate 041-8611, Japan
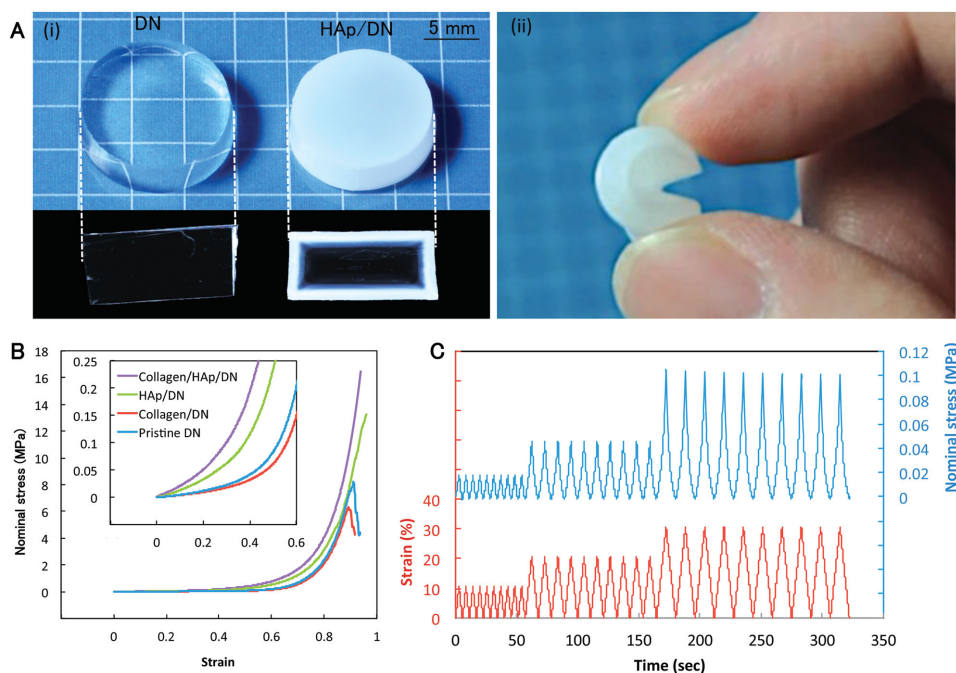
Figure 1. The appearance and mechanical properties of HAp/DN hydrogel. A) By mineralizing HAp in the DN gel, the gel changed its appearance from transparent (DN gel) to turbid (HAp/DN gel); i) The cut cross-section image shows a HAp/gel layer about 500 μm thick for a dipping time $t = 110$ s and dipping cycle $n = 5$. ii) The HAp/DN gel maintained the high flexibility. B) Compressive stress–strain curves of HAp/DN, pristine DN, collagen/DN, and collagen/HAp/DN gels, and the inserted figure is the enlarged view of the low strain region. C) Repeated compressive tests of HAp/DN for ten times at each strain; 10%, 20%, and 30%.

of the HAp/DN gel was owing to the formation of a gel/bone hybrid layer at the interface with gradient structure.

As a typical tough hydrogel, we used a DN gel consisting of poly(2-acrylamido-2-methyl propanesulfonic acid) as the brittle first network and poly(N,N-dimethylacrylamide) (PDMAAm) as the ductile second network.[3] The DN gel from this combination has shown excellent mechanical and biological performances, including high strength and toughness, biocompatibility, low wearing ability against repeated sliding, and ability to induce regeneration of hyaline cartilage in vivo.[3,17–19]

To carry out low-crystallinity HAp mineralization on the surface layer of the DN gel, we alternatively dipped the DN gel in aqueous solutions of calcium chloride ($CaCl_2$) and dipotassium hydrogen phosphate (K_2HPO_4).[20,21] After repeated dipping, the transparent DN gel gradually became opaque white (**Figure 1**A(i)) with only slight shrinkage in volume (Figure S1A,B, Supporting Information). Cross-sectional images showed that HAp was mineralized on the surface layer of the hydrogels (Figure 1A(i)). The thickness of the HAp layer could be controlled by the dipping time t (Figure S1C,D, Supporting Information), and the HAp content in the layer could be controlled by the dipping cycle n. For conditions $t = 110$ s and $n = 5$, we obtained an HAp/DN gel having a 500 μm-thick hybrid layer on its surface; the composition of this layer was 4.1 wt% mineral, 8.2 wt% polymer, and 87.7 wt% water (**Table 1**). X-ray diffraction revealed that characteristic peaks for the HAp crystal appeared over $n = 3$, and their intensities increased with increase in n, owing to the ripening from amorphous to crystals (Figure S2, Supporting Information).[20]

The surface of the HAp/DN gel was as smooth as that of the pristine DN gel, and its contact angle to water (CAW) gradually increased with cycle n; at $n = 5$, the CAW was almost equal to that of the sintered HAp plate (Figure S3 (Supporting Information), and Table 1). Furthermore, the zeta potential of the HAp/DN at pH 5.5 changed from the pristine value to almost the same as that of the sintered HAp plate (Table 1).

The HAp/DN gel maintained its original soft, pliable nature (Figure 1A(ii), Movie S1, Supporting Information). It showed improved mechanical properties in the compression test compared with the pristine DN gel (Figure 1B). Both the pristine and HAp/DN gels did not fail, even at a compressive strain ε as high as 0.9; indeed, the Young's modulus and the stress at $\varepsilon = 0.9$ of the mineralized sample were higher than those of the pristine (Table 1). The toughness in terms of work of compression at $\varepsilon = 0.9$ of the HAp/DN gel was about 1.5 times higher than that of the pristine (Table 1). The tensile test also showed an enhanced Young's modulus but the fracture strain became slightly lower than that of the pristine sample (Figure S4A, Supporting Information). These mechanical property changes cannot be explained by the slight dehydration of the sample, and they indicate the crosslinking effect of HAp, which reinforces the DN at the cost of reducing the extensibility of the polymer network. The repeated compression test showed no changes in the mechanical performance with the compression cycle both for the HAp/DN gel and the DN gel (Figure 1C; Figure S4B, Supporting Information).

To confirm that the DN gel is permeable to collagen molecules, which are the main protein components of bone, we immersed the DN gel in a 1.5 wt% solution of triple-helix collagen molecules, and the amount of collagen permeation was

Table 1. Summary of compositions, surface analysis, and mechanical properties of the pristine DN gel, HAp/DN gel, sintered HAp plate, collagen/DN gel, and collagen/HAp/DN gel. The composition and mechanical properties were estimated by thermogravimetry and compressive/tensile tests, respectively. Work of compression and work of extension were estimated from the area under the stress–strain curve of Figure 1B. The error ranges are standard deviation from the data of three samples.

Sample		DN	HAp/DN[a]	Sintered HAp	Collagen/DN[b]	Collagen/HAp/DN[a,b]
Composition [wt%]	Water	92	87.7	0.0	92.4	88.7
	Polymer	8.0	8.2	0.0	7.6	7.1
	Mineral	0.0	4.1	100	0.0	4.2
Contact angle of water [°]		47 ± 6	101 ± 3	103 ± 2	–	–
Zeta potential [mV]		−8.27 ± 1.23	−18.0 ± 2.43	−17.4 ± 2.11	–	–
Young's modulus[c] [MPa]		0.035 ± 0.004	0.084 ± 0.004	414 ± 4	0.039 ± 0.001	0.186 ± 0.005
Stress at $\varepsilon = 0.9$[c] [MPa]		7.39 ± 0.48	9.50 ± 1.54	–	5.92 ± 0.21	11.25 ± 0.12
Work of compression[c] [MJ m^{-3}]		0.67 ± 0.49	1.04 ± 0.18	–	0.68 ± 0.03	1.71 ± 0.01
Young's modulus[d] [MPa]		0.074 ± 0.001	0.159 ± 0.008	–	–	–
Fracture stress[d] [MPa]		0.61 ± 0.03	0.45 ± 0.03	–	–	–
Fracture strain[d] [mm mm^{-1}]		3.23 ± 0.36	1.64 ± 0.19	–	–	–
Work of extension[d] [MJ m^{-3}]		1.08 ± 0.19	0.35 ± 0.09	–	–	–

[a]Dipping time t = 110 s, mineralization cycle n = 5; [b]Collagen concentration in gel was 1.5 wt% as determined by UV–vis absorbance; [c]Measured by compressive test; [d]Measured by tensile test.

measured by UV–visible light spectroscopy. The absorbance of the characteristic collagen peak increased with soaking time, and the diffusion reached equilibrium at around 56 h (Figure S5A,B, Supporting Information). The transparent DN gel became slightly opaque and white, indicating collagen-fibril formation in the gel at the prolonged time (Figure S5C, Supporting Information).[22] To see if deposition of HAp nanocrystals would lead to the formation of a nanocomposite with collagen in the DN gel, HAp mineralization was then performed for the collagen-penetrated DN gel. We selected transparent collagen/DN gel samples containing 1.5 wt% collagen for HAp mineralization. The compressive mechanical properties of the collagen/DN gel and collagen/HAp/DN gel were evaluated (Figure 1B and Table 1). The stress–strain curve of the collagen/DN gel almost overlapped with that of the pristine DN gel, indicating that the mere penetration of collagen into the DN gel brings negligible change in the mechanical strength. By contrast, a remarkable enhancement of the mechanical strength was observed after HAp mineralization of the collagen/DN gel. In fact, the collagen/HAp/DN gel showed even higher strength than that of the HAp/DN gel. Just like the HAp/DN gel, the collagen/HAp/DN gel also did not show failure even at maximum compression. Therefore, deposition of HAp nanocrystals reinforced the collagen/DN gel substantially by forming nanocomposite with collagen. It is likely that the collagen molecules form the third interpenetrating network structure that is crosslinked by HAp particles. Also, collagen molecules form some bundles or aggregations in the DN gel because the pristine gel became opaque after collagen diffusion, as shown in Figure S5C (Supporting Information).

To test the in vivo osteointegration, we created a cylindrical gel plug covered by a 500 μm-thick HAp hybridized layer and implanted the plug into an osteochondral defect created in the rabbit femoral groove (**Figure 2**A). Figure 2B shows microcomputed tomography (μCT) images of the osteochondral defects with the pristine DN (i–ii) and HAp/DN (iii–iv) at

four weeks after implantation. The HAp-layered region of the HAp/DN gel was clearly recognizable from the surrounding tissue in (iii), as indicated by the red arrow. iv) Furthermore, the HAp/DN layer completely coalesced with the surrounding bone tissue, as revealed by the sagittal plane image. iv) Comparing the sagittal plane images of the HAp/DN gel with those of the pristine (ii), more osteogenesis was observed around the HAp/DN gel than around the pristine.

We designed a push-out test to measure the bonding strength of the HAp/DN gel to the rabbit bone for different implantation times (Figure 2C). As shown in Figure 2D, the pristine DN gel showed a very low push-out load, both at one week and four weeks implantation. By contrast, the push-out load of HAp/DN gel at one week was as low as that of pristine but increased dramatically at four weeks. Actually, the bonding was so strong at four weeks that the HAp/DN gel matrix ruptured before being pushed out, and the maximum load shown in Figure 2D is the result of rupture of the HAp/DN gel, not the failure of bonding. Some parts of the gel matrix, which were strongly adhered to the internal wall of the bone tissue, remained in the defect. The push-out test may demonstrate a complex state of the interface stress. However, it was attempted to estimate roughly the order of bonding stress. From the value of maximum load/cylindrical surface area, we knew that the true shear bonding stress might be larger than 0.6 MPa. This value was comparable to the reported bonding strength of a smooth and pure HAp to bone (0.15 MPa) at eight weeks.[23] Thus, the HAp/DN gel showed strong osteointegration, while the pristine DN gel did not.

To clarify the structure to show the strong bonding, first, we stained the implanted samples using anionic methyl blue, which forms a complex with the cationic moieties of the proteins.[24] As shown in Figure 2E, the nonimplanted HAp/DN gel was not stained at all due to absence of any proteins (Figure 2E(i),(ii)). By contrast, for the four-weeks-implanted DN and HAp/DN gels, the edge regions were clearly stained with blue color
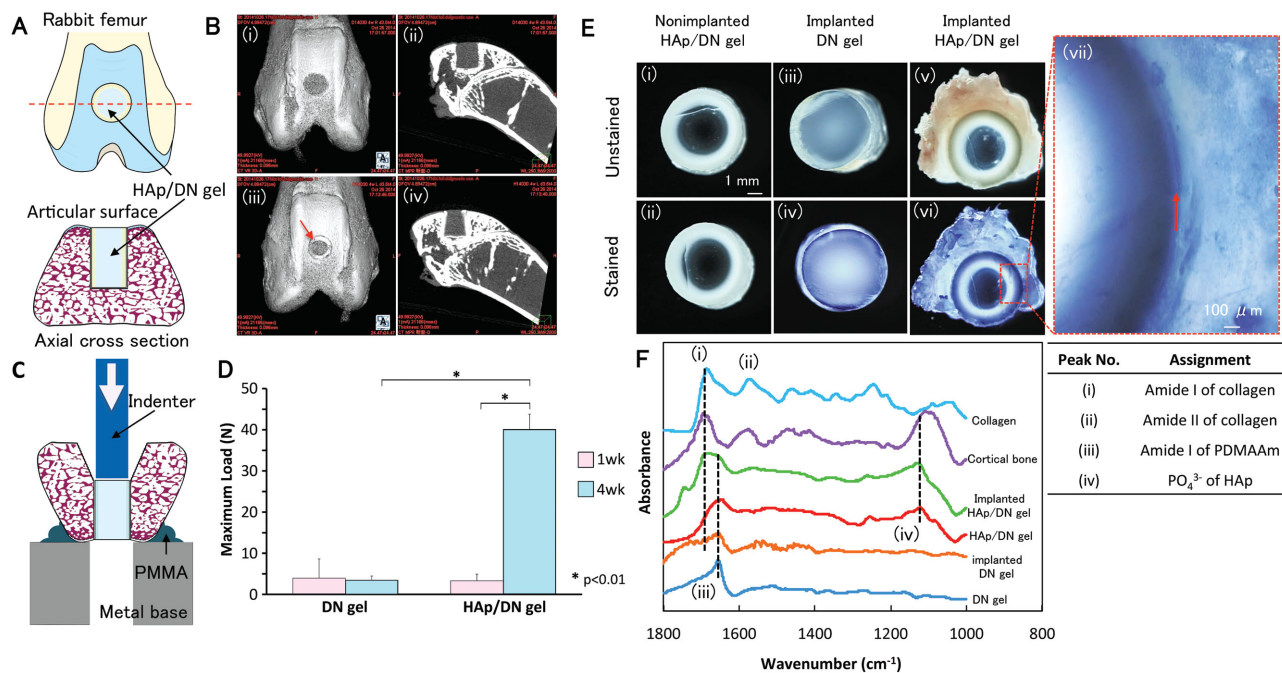
Figure 2. In vivo results of bonding strength and protein diffusion. A) Schematic of HAp/DN gel plugs implanted in rabbit femurs. B) i,ii) μCT of DN or iii,iv) HAp/DN gels four weeks post-implantation. C) Set up of the push-out test for measuring the bonding strength of the gels to bone. The femur specimens were fixed on a hollow metal base by a poly(methyl methacrylate) (PMMA) resin, and the gel was pushed by an indenter. D) Maximum load required to push-out the pristine DN gel and HAp/DN gel implanted for one week and four weeks. Data were means and standard deviations for five samples. The mean value was statistically compared among the groups using two-way analysis of variance (ANOVA) with the Tukey's honest significant difference test for post-hoc multiple comparisons. Probability values less than 0.05 were considered significant. E) i,ii) Stereoscopic images of nonimplanted HAp/DN gel, iii,iv) four weeks implanted DN, and v,vi,vii) HAp/DN gels before (i,iii,v) and after (ii,iv,vi) staining by methyl blue. vii) is the enlarged image of (vi) at the boundary. The red arrow indicates the position for the seamless wide-range FE-TEM observation in Figure 3. F) IR spectra of DN, implanted DN, HAp/DN, implanted HAp/DN gels, cortical bone, and collagen from rat tails. The peaks in the figure are assigned in the table on the right.

(Figure 2E(iii),(iv),(v),(vi)), indicating the diffusion of proteins into these gels. For the sample of the HAp/DN gel that strongly bonded to the bone, the surrounding bone tissue was also stained, but only slightly. This is because the presence of dense HAp prevents the staining of collagens in the bone. Comparing with the DN gel, the HAp/DN gel showed wider and denser straining, suggesting the presence of more proteins in the HAp/DN gel. The high-magnification image of the HAp/DN sample further revealed that the proteins at the gel–bone interface had a gradient distribution of ≈500 μm width (Figure 2E(vii)).

It is likely that many proteins from the surrounding serum diffused into the gel and were stained by methyl blue. To verify the presence of collagen, we further characterized the dried specimens with microscopic reflection infrared (IR) spectroscopy (Figure 2F). The collagen shows characteristic peaks at 1693 and 1559 cm⁻¹ assigned to amide I and II, respectively.[25] These two peaks were clearly observed for pure collagen solution and cortical bone of the femur. On the other hand, for non-implanted samples, both the pristine and HAp/DN gel showed a peak at 1654 cm⁻¹, assigned to amide I of the second network of the DN gel, PDMAAm. The four-weeks-implanted HAp/DN gel exhibited one broad peak around the amide I region (1693–1654 cm⁻¹); this peak could be deconvoluted into two peaks assigned to amide I of collagen and PDMAAm, respectively (Figure S6, Supporting Information). This result suggests the presence of collagens in the HAp/DN gel. By contrast, the implanted DN gel showed a weak and broad shoulder in

the 1654–1700 cm⁻¹ region, indicating that various kinds of proteins are present in the DN gel. Considering the relative peak intensity of the deconvolution, the weakness of the amide II peak of the implanted HAp/DN gel compared with those of standard collagen and cortical bone, was reasonable. In addition, the IR profile also showed a characteristic peak of PO_4^{3-} of HAp at around 1100 cm⁻¹[26] for the HAp/DN gels but not for the DN gels, both non-implanted and implanted.

By field-emission transmission electron microscopy (FE-TEM), the morphologies of HAp before and after implantation were clearly observed. The seamless wide-range FE-TEM image of non-implanted HAp/DN showed the dispersed distribution of the HAp nanocrystals with spiny spherical shape measuring ≈200–600 nm in diameter (**Figure 3**A–D). The outermost layer of the HAp/DN gel was almost covered with the HAp nanocrystals (Figure 3E). The diffraction spots in Figure 3B(iii)–E(iii) confirm the crystalline structure of the spiny spherical HAp nanoparticles. On the other hand, the seamless wide-range FE-TEM image of implanted HAp/DN at the boundary region (indicated by the red arrow in Figure 2E(vii)) showed a gradient distribution of HAp with no clear boundary between the gel and the bone tissue (Figure 3F). Dispersed HAp nanospheres of similar density as that of the non-implanted HAp/DN gel were observed in the gel region far from the interface to bone. However, the density of the HAp nanospheres remarkably increased and continuous HAp structure was observed in the region close to the bone, indicating that some HAp was newly formed. The FE-TEM images at a high

**ADVANCED
MATERIALS**

www.advmat.de

*Materials
Views*

www.MaterialsViews.com
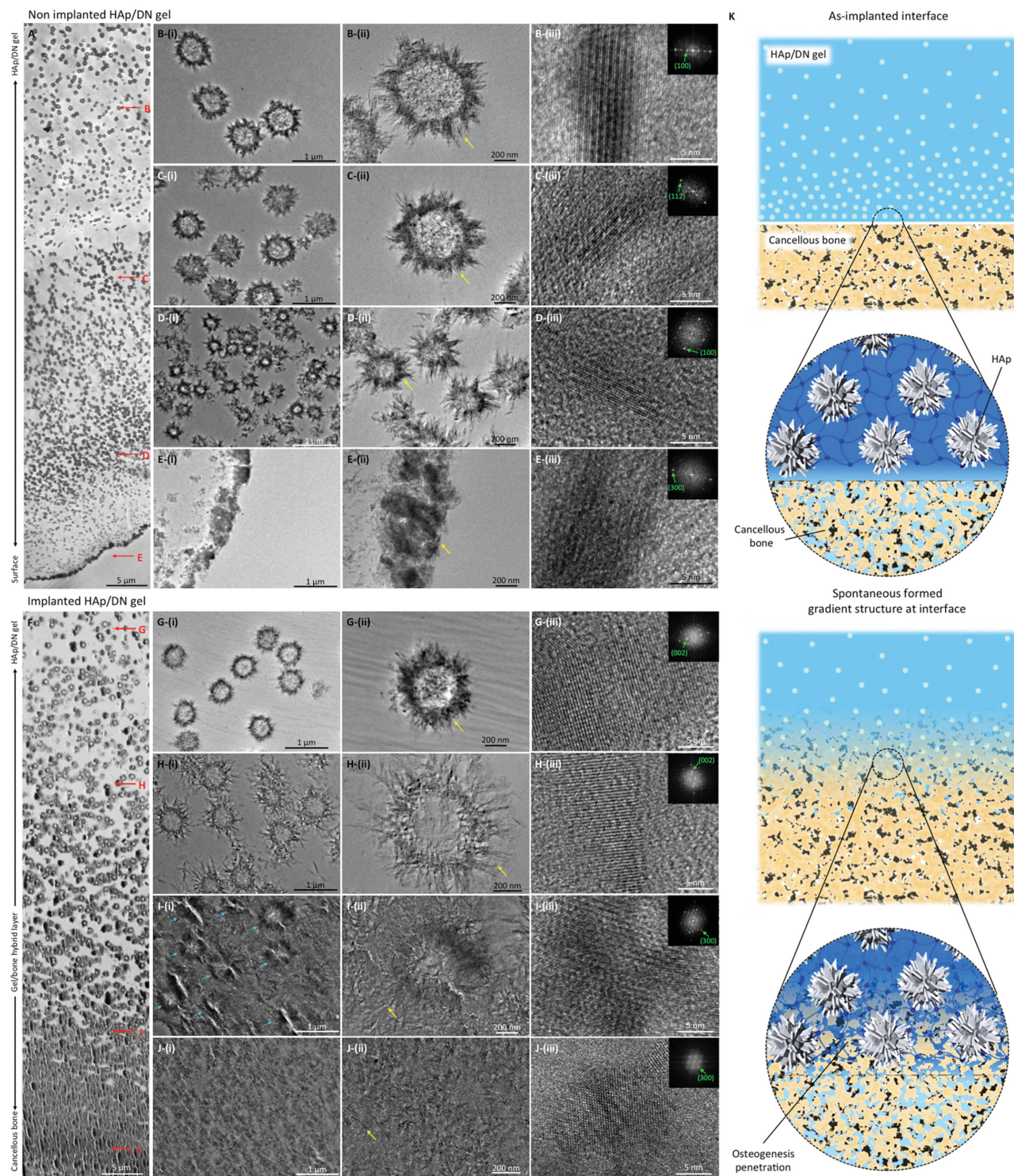
Figure 3. Gel/bone interface structures of the gels implanted in an osteochondral defect created in the rabbit femoral groove. A) Seamless wide-range FE-TEM image of nonimplanted HAp/DN gel ($t = 110$ s, $n = 5$) from the surface (lower) to the bulk (upper) of the sample. B–E are the high magnificent images in positions indicated by the red arrows in (A). F) Seamless wide-range image of HAp/DN gel four weeks post-implantation from the bone (lower) to the gel (upper) of the sample. G–J are the high magnificent images in positions indicated by the red arrows in (F). The yellow arrows in (ii) indicate observation positions of images in (iii). Magnification is: i) 6000×, ii) 15 000×, and iii) 600 000×. The inset images in (iii) are selected-area 2D fast Fourier transform of the images. The diffraction spots in (iii) confirm the crystalline structure of the spiny spherical HAp nanoparticles. K) Schematic illustration for robust bonding of the HAp/DN gel to bone by osteogenesis penetration.

magnification further showed that the HAp nanospheres located in the gel region far from the interface also had the spiny spherical morphology (Figure 3G), similar to that of non-implanted HAp/DN (Figure 3B–D). However, near the bone side, some new HAp was observed on the whisker-like surface of the spiny HAp nanospheres (Figure 3H). In the region quite close to the bone tissue, ripened new HAp with morphology similar to bone tissue infilled the space and completely coalesced with the spiny HAp nanocrystals (Figure 3I,J). The diffraction spots in Figure 3G(iii)–J(iii) also confirm the crystalline structure of the HAp. It is clearly indicated that osteogenesis penetrated into semi-permeable DN gel, although any cells are too large to penetrate into the gel matrix. From the results of Figure 3F, the transition layer of HAp was about ≈40 µm in width, which is about 1/10 of the protein staining width as observed in Figure 2E. As the pre-existed HAp nanocrystals almost maintained the same density and morphology after the formation of the bonding, the observed HAp gradient layer was not due to the reconstruction of the pre-existed nanocrystals, but rather due to the additional mineral sources migrated into the hydrogel. By contrast, such new HAp formation was not found in the four-weeks-implanted pristine DN gel (Figure S7, Supporting Information). The above results indicate that the HAp nanocrystals in the HAp/DN gel are able to induce the spontaneous osteogenesis inside the gel to form the gel/bone hybrid layer, as illustrated in Figure 3K. This hybrid layer that gradually changed from gel-rich phase to bone-rich phase should be responsible for the strong bonding of the HAp/DN gel to the bone. Since no gel/bone hybrid layer was formed for the pristine DN gel, such osteogenesis was activated by the HAp nanocrystals pre-existing in the DN gel. A possible mechanism is that dissolution of a small amount of HAp nanocrystals stimulates the cells on the bone region to perform osteogenesis.[11] During this process, biosynthesized collagens and minerals diffused into the gel matrix to form the gel/bone layer. This bonding mechanism of the HAp/DN gel to bones is quite different from that of solid materials, such as metal alloys and ceramics via the osteoconductive HAp layer.[10] In the latter case, the HAp layer forms sharp interface with bone.

Thus, the DN gel containing HAp nanocrystals showed high osteointegration as a result of spontaneous formation of a gel/bone hybrid layer at the interface, owing to the semipermeable characteristics of the hydrogel and the osteoconduction of HAp. Since the HAp mineralization to form nanocrystals is independent of the specific chemistry of the polymer network, but only depends on the semipermeable nature of the hydrogels, this strong bonding approach could be applicable to a variety of biomaterial-based tough hydrogels. We expect that these results will promote the potential application of tough hydrogel materials as cartilages. This result will also merit the development of hydrogel-based artificial ligaments in the future.

Experimental Section

Experimental details are provided in the Supporting Information.

Supporting Information

Supporting Information is available from the Wiley Online Library or from the author.

[1] B. R. Mandelbaum, J. E. Browne, F. Fu, L. Micheli, J. B. Mosely Jr., C. Erggelet, T. Minas, L. Peterson, *Am. J. Sport Med.* **1998**, *26*, 853.

[2] J. A. Buckwalter, H. J. Mankin, *Arthritis Rheum.* **1998**, *41*, 1331.

[3] J. P. Gong, Y. Katsuyama, T. Kurokawa, Y. Osada, *Adv. Mater.* **2003**, *15*, 1155.

[4] T. L. Sun, T. Kurokawa, S. Kuroda, A. B. Ihsan, T. Akasaki, K. Sato, Md. A. Haque, T. Nakajima, J. P. Gong, *Nat. Mater.* **2013**, *12*, 932.

[5] J. Y. Sun, X. Zhao, W. R. K. Illeperuma, O. Chaudhuri, K. H. Oh, D. J. Mooney, J. J. Vlassak, Z. Suo, *Nature* **2012**, *489*, 133.

[6] S. Y. Yang, E. D. O'Cearbhaill, G. C. Sisk, K. M. Park, W. K. Cho, M. Villiger, B. E. Bouma, B. Pomahac, J. M. Karp, *Nat. Commun.* **2013**, *4*, 1702.

[7] S. Rose, A. Prevoteau, P. Elzière, D. Hourdet, A. Marcellan, L. Leibler, *Nature* **2014**, *505*, 382.

[8] J. P. Gong, *Soft Matter* **2006**, *2*, 544.

[9] K. Matsuo, N. Irie, *Arch. Biochem. Biophys.* **2008**, *473*, 201.

[10] L. M. Sun, C. C. Berndt, K. A. Gross, A. Kucuk, *J. Biomed. Mater. Res.* **2001**, *58*, 570.

[11] Y. Gonda, K. Ioku, Y. Shibata, T. Okuda, G. Kawachi, M. Kamitakahara, H. Murayama, K. Hideshima, S. Kamihira, I. Yonezawa, H. Kurosawa, T. Ikeda, *Biomaterials* **2009**, *30*, 4390.

[12] Y. L. Chang, D. Lew, J. B. Park, J. C. Keller, *J. Oral Maxil. Surg.* **1999**, *57*, 1096.

[13] M. Thorwarth, S. Schultze-Mosgau, P. Kessler, J. Wiltfang, K. A. Schlegel, *J. Oral Maxil. Surg.* **2005**, *63*, 1626.

[14] J. Watanabe, M. Akashi, *Biomacromolecules* **2006**, *7*, 3008.

[15] P. Bornstein, W. Traub, in *The Proteins*, (Ed: H. Neurath, R. L. Hill), Academic Press, New York **1979**.

[16] P. G. Gennes, *Scaling Concepts in Polymers Physics*, Cornell University Press, Ithaca, NY, USA **1979**.

[17] Y. Tanabe, K. Yasuda, C. Azuma, H. Taniguro, S. Onodera, A. Suzuki, Y. M. Chen, J. P. Gong, Y. Osada, *J. Mater. Sci., Mater. M.* **2008**, *19*, 1379.

[18] K. Yasuda, J. P. Gong, Y. Katsuyama, A. Nakayama, Y. Tanabe, E. Kondo, M. Ueno, Y. Osada, *Biomaterials* **2005**, *26*, 4468.

[19] K. Yasuda, N. Kitamura, J. P. Gong, K. Arakaki, H. J. Kwon, S. Onodera, Y. M. Chen, T. Kurokawa, F. Kanaya, Y. Ohmiya, Y. Osada, *Macromol. Biosci.* **2009**, *9*, 307.

[20] T. Taguchi, A. Kishida, M. Akashi, *Chem. Lett.* **1998**, *27*, 711.

[21] T. Nonoyama, M. Tanaka, T. Kinoshita, F. Nagata, K. Sato, K. Kato, *Chem. Commun.* **2010**, *46*, 6983.

[22] D. J. S. Hulmes, *J. Struct. Biol.* **2002**, *137*, 2.

[23] J. T. Edwards, J. B. Brunski, H. W. Higuchi, *J. Biomed. Mater. Res.* **1997**, *36*, 454.

[24] S. Sigurgisladottir, M. S. Sigurdardottir, H. Ingvarsdottir, O. J. Torrissen, H. Hafsteinsson, *Aquac. Res.* **2001**, *32*, 1.

[25] E. P. Paschalis, R. Mendelsohn, A. L. Boskey, *Clin. Orthop. Relat. Res.* **2011**, *469*, 2170.

[26] L. B. Cimdina, N. Borodajenko, *Infrared Spectroscopy - Materials Science, Engineering and Technology*, (Ed: T. Theophanides), InTech, Rijeka, Croatia **2012**.